PERGAMON

Available online at www.sciencedirect.com

SCIENCE DIRECT®

Polyhedron 22 (2003) 133–143

POLYHEDRON

www.elsevier.com/locate/poly

Preparation and crystal structures of Mn^{II}, mixed-valent Mn^{II}/Mn^{III}, and Mn^{III} polymeric compounds

Anastasios J. Tasiopoulos, Nicholas C. Harden, Khalil A. Abboud, George Christou *

Department of Chemistry, University of Florida, Gainesville, FL 32611-7200, USA

Received 16 July 2002; accepted 22 August 2002

Abstract

The preparation and crystal structures of three polymeric Mn compounds are reported. The comproportionation reaction between $Mn(OAc)_2\cdot 4H_2O$ and $KMnO_4$ in MeOH–AcOH (2:3) leads to isolation of $\{[Mn(OH)(OAc)_2]\cdot AcOH\cdot H_2O\}_n$ (**1**). The structure consists of chains of $[Mn(\mu\text{-}OH)(\mu\text{-}OAc)_2Mn]$ triply-bridged units. The chains are linked into 3D networks by hydrogen-bonding interactions involving the AcOH and H_2O molecules of crystallization. Oxidation of $[Mn_{12}O_{12}(O_2CPh)_{16}(H_2O)_4]$ by controlled potential electrolysis in CH_2Cl_2 with $NBu^n_4PF_6$ as supporting electrolyte yields a brown solution which slowly turns purple and then pale yellow. Deep purple crystals, obtained by addition of hexanes, were identified crystallographically as $\{(NBu^n_4)[Mn_2(O_2PF_2)_6]\cdot 2/3CH_2Cl_2\}_n$ (**2**), which is mixed-valent and consists of a chain of $[Mn^{II}(\mu\text{-}O_2PF_2)_3Mn^{III}]$ triply-bridged units. Bond distances, bond valence sum calculations, and a Jahn–Teller (JT) axial elongation at the Mn^{III} sites confirm a trapped-valence situation. Dissolution of $Mn(OAc)_2\cdot 4H_2O$ in EtOH results in a subsequent crystallization of a white solid analyzing as $[Mn(OAc)_2\cdot 3/8H_2O]$ (**3a**). Crystals grown from MeOH–Et_2O were structurally identified as $[Mn_4(OAc)_8(MeOH)_2]_n$ (**3b**), and consist of Y-shaped Mn_4 units bridged by AcO^- groups to give a 3D network. Variable-temperature, solid-state magnetic susceptibility studies establish that **1**, **3a** and **3b** are antiferromagnetically coupled to give diamagnetic ground states.

Keywords: Crystal structures; Polymeric; Mn compounds; Solid state

1. Introduction

We have for many years been interested in the synthesis of polynuclear Mn clusters, primarily with carboxylate ligation and often with bridging oxide ions. We have particularly sought molecular species and, indeed, polymeric products have been the exception rather than the rule in our work. Our efforts have been stimulated by two primary reasons: (i) the photosynthetic water-oxidizing complex (WOC) of green plants and cyanobacteria contains a Mn_4 unit with primarily carboxylate ligation [1,2]. Thus, synthetic Mn_4 molecular clusters have been sought as models of the WOC [3–7]; and (ii) Mn clusters often possess large, and sometimes abnormally large ground state spin (S) values, and some of them have proved to be single-molecule magnets; these are molecular species with the ability to function as nanoscale magnetic particles [8–11]. For this reason, we are actively developing methods to high-nuclearity molecular species that might be new SMMs.

Work to date has resulted in molecular species with nuclearities up to 30 and metal oxidation states in the II–IV range, including mixed valency [12–15]. As mentioned, polymeric materials have surprisingly rarely been encountered (with the trivial exception of Mn oxides), but we have occasionally come across some. In this paper, we report three such polymeric materials that were obtained unintentionally during some of our many efforts to prepare molecular species. The polymers are at the Mn^{II}, mixed-valent Mn^{II}/Mn^{III}, and Mn^{III} oxidation states.

* Corresponding author. Tel.: +1-352-392-8314; fax: +1-352-392-8757

E-mail address: christou@chem.ufl.edu (G. Christou).

0277-5387/02/$ - see front matter
PII: S0277-5387(02)01262-7

2. Experimental

2.1. Compound preparation

All manipulations were performed under aerobic conditions with the use of materials as received unless otherwise indicated; water was distilled in-house. $[Mn_{12}O_{12}(O_2CPh)_{16}(H_2O)_4]\cdot PhCO_2H\cdot CH_2Cl_2$ was synthesized according to the literature preparation [16]. Elemental analyses were performed by Atlantic Microlab, Inc (Norcross, GA), and by the in-house facilities of the Chemistry Department, University of Florida.

2.1.1. Preparation of $\{[Mn(OH)(OAc)_2]\cdot AcOH\cdot H_2O\}_n$ (1)

To a slurry of $Mn(OAc)_2\cdot 4H_2O$ (4.04 g, 16.5 mmol) in MeOH–AcOH (8/12 ml) was slowly added a solution of $KMnO_4$ (1.00 g, 6.33 mmol) in MeOH–AcOH (8/12 ml), resulting in a dark reddish-brown solution. The solution was stirred for 0.5 h, filtered, and the filtrate maintained at room temperature. After 10 days, reddish-brown crystals were collected by filtration, washed with EtOH (2×15 ml), and copious Et_2O, and dried in air. The yield was 0.95 g (16% based on total Mn). *Anal*. Calc for $C_6H_{13}O_8Mn$: C, 26.88; H, 4.89; Mn, 20.49. Found: C, 26.60; H, 4.75; Mn, 20.70%. Selected IR data (KBr, cm^{-1}): 3362 (s, br), 2945 (m), 1701 (s), 1549 (s), 1425 (s), 1399 (s), 1350 (m), 1340 (w), 1277 (m), 1146 (w), 1040 (m), 1019 (m), 989 (w), 962 (w), 941 (w), 887 (w), 676 (m), 620 (m), 562 (s), 459 (w), 437 (w).

2.1.2. Preparation of $\{(NBu^n_4)[Mn_2(O_2PF_2)_6]\cdot 2/3CH_2Cl_2\}_n$ (2)

$[Mn_{12}O_{12}(O_2CPh)_{16}(H_2O)_4]\cdot PhCO_2H\cdot CH_2Cl_2$ (0.21 g, 0.08 mmol) was dissolved in CH_2Cl_2 (80 ml) containing 0.1 M $NBu^n_4PF_6$ as supporting electrolyte. The solution was electrolyzed at a potential of +1.07 V versus the Fc^+–Fc couple in an effort to produce the singly oxidized species, $[Mn_{12}O_{12}(O_2CPh)_{16}(H_2O)_4]^+$. After current corresponding to 1 mol equiv. of coulombs per Mn_{12} had been passed, the dark brown solution was filtered and layered in crystallizing tubes with hexanes. After 3 weeks, the solution in several of the tubes had turned a purple color and in one case deep-purple X-ray quality crystals of **2** had formed. IR: ν_{asym} (PO_2) 1296 cm^{-1}; ν_{sym} (PO_2) 1159 cm^{-1}; ν (PF) 884 cm^{-1}; δ (PO_2) 558 cm^{-1}; δ (POF) 497 cm^{-1}. The small amount of available crystalline solid and the limited stability of the material prevented elemental analysis.

2.1.3. Dissolution of $Mn(OAc)_2\cdot 4H_2O$ in EtOH: $[Mn(OAc)_2\cdot 3/8H_2O]$ (3a)

$Mn(OAc)_2\cdot 4H_2O$ (1.00 g, 4.08 mmol) was dissolved in anhydrous EtOH (20 ml) to give a homogeneous solution. After 10–15 min, a white microcrystalline precipitate began to slowly form. When precipitation was judged complete, the white solid was collected by filtration, washed well with EtOH and Et_2O, and dried in air; the yield was typically 0.67 g (90%). Samples filtered under nitrogen and dried under vacuum analyzed for $Mn(OAc)_2\cdot 3/8H_2O$, or $Mn_4(OAc)_8(H_2O)_{1.5}$. *Anal.* Calc for $C_{16}H_{27}O_{17.5}Mn_4$: C, 26.72; H, 3.78. Found: C, 26.70; H, 3.75%. Samples exposed to air slowly absorbed moisture and analyzed for $Mn(OAc)_2\cdot 1/2H_2O$, or $Mn_4(OAc)_8(H_2O)_2$. *Anal.* Calc for $C_{16}H_{28}O_{18}Mn_4$: C, 26.39; H, 3.88. Found: C, 26.36; H, 4.05%.

2.1.4. Dissolution of $Mn(OAc)_2\cdot 4H_2O$ in MeOH: $[Mn_4(OAc)_8(MeOH)_2]_n$ (3b)

$Mn(OAc)_2\cdot 4H_2O$ (1.10 g, 4.49 mmol) was dissolved in anhydrous MeOH (15 ml) under an argon atmosphere using standard inert-atmosphere techniques. To the homogeneous solution was added Et_2O (75 ml), which caused the immediate precipitation of a fine white precipitate. When precipitation was judged complete, the solid was collected by filtration under aerobic conditions, washed well with Et_2O, and dried in air; the yield was 0.73 g (85%). The isolated material is hygroscopic. Material dried under vacuum but stored in air analyzed for $Mn_4(OAc)_8(H_2O)_4$. *Anal*. Calc for $C_{16}H_{32}O_{20}Mn_4$: C, 25.15; H, 4.22. Found: C, 25.22; H, 4.53%.

A crystal suitable for crystallography was obtained by adding Et_2O to a small scale MeOH reaction solution until turbidity just began to appear. The solution was then left undisturbed overnight. This gave well-formed, colorless needles of $[Mn_4(OAc)_8(MeOH)_2]_n$, and these were kept in contact with their mother liquor until a suitable crystal had been chosen, transferred to the goniometer, and cooled for characterization and data collection.

2.2. Crystallography

Data for complexes **1** and **2** were collected at 193 K on a Siemens SMART PLATFORM diffractometer equipped with a CCD area detector and a graphite monochromator utilizing Mo Kα radiation ($\lambda = 0.71073$ Å). Data collection parameters are listed in Table 1. Cell parameters were refined using up to 8192 reflections. A full sphere of data (1381 frames) was collected using the ω-scan method (0.3° frame width). The first 50 frames were re-measured at the end of data collection to monitor instrument and crystal stability (maximum correction on I was $<1\%$). An absorption correction by integration was applied, based on the measured indexed crystal faces.

The structures were solved by the Direct Methods procedures in SHELXTL5, and refined using full-matrix least squares. Non-hydrogen atoms were refined aniso-

Table 1
Crystallographic data for complexes **1**, **2**, and **3b**

	1	**2**	**3b**
Formula	$C_6H_{13}MnO_8$	$C_{50}H_{112}Cl_4F_{36}Mn_6N_3O_{36}P_{18}$	$C_{18}H_{32}O_{18}Mn_4$
Formula weight, (g mol^{-1})	268.10	3044.33	756.21
Space group	$P2_1/m$	$Pna2_1$	$P2_1$
a (Å)	7.9382(6)	17.550(2)	8.402(2)
b (Å)	6.7675(5)	35.768(3)	15.916(4)
c (Å)	10.9173(8)	18.945(2)	11.136(3)
β (°)	106.726(2)	90	93.12(1)
V (Å^3)	561.68(7)	11 892(2)	1487(1)
Z	2	4	2
T (°C)	−80	−80	−171
Radiation	Mo Kα	Mo Kα	Mo Kα
ρ_{calc}, (g cm^{-3})	1.585	1.700	1.69
μ (mm^{-1})	1.195	1.074	1.656
R or R_1 [a,b]	3.06	5.73	7.27
R_w [b,c] or wR_2 [b,d]	6.59 [d]	14.62 [d]	7.13 [c]

[a] $R = R_1 = 100\Sigma(||F_o|-|F_c||)/\Sigma|F_o|$.
[b] $I > 2\sigma(I)$.
[c] $R_w = 100[\Sigma w(|F_o|-|F_c|)^2/\Sigma w|F_o|^2]^{1/2}$, where $w = 1/\sigma^2(|F_o|)$.
[d] $wR_2 = 100[\Sigma w(F_o^2-F_c^2)^2/\Sigma[w(F_o^2)^2]]^{1/2}$, $w = 1/[\sigma^2(F_0^2)+(ap)^2+bp]$, where $p = [\max(F_o^2, 0)+2F_c^2]/3$.

tropically, whereas the hydrogen atoms were placed in ideal, calculated positions, with isotropic thermal parameters riding on their respective carbon atoms. For **1**, the water and hydroxyl hydrogen atoms, all of which are involved in H bonding, were obtained from a difference Fourier map and refined without any constraints. A total of 184 parameters were refined in the final cycles of refinement on F^2. For **2**, some disorder was observed in a PF_2 unit, where the F atoms were resolved but the disorder in the P position could not be resolved. Also, one $NBu^n_4{}^+$ cation displayed disorder in two of its butyl groups. Each disorder was refined in two parts with their site occupancy factors dependently refined. A total of 1374 parameters were refined in the final cycles of refinement on F^2.

Data for complex **3b** were collected on a Picker four-circle diffractometer at the Indiana University Molecular Structure Center. Data collection parameters are listed in Table 1. Several attempts were required to properly determine the phases by direct methods (MULTAN). The correct solution was finally determined by eliminating all h0l data from the normalized structure factors. The resulting phased E-map revealed the location of three of the four Mn atoms. Subsequent Fourier techniques located the remaining non-hydrogen atoms. Many of the hydrogen atoms were visible in a difference Fourier map phased on the non-hydrogen atoms and were included as isotropic contributors in the final cycles of refinement on F; non-hydrogen atoms were refined with anisotropic thermal parameters. The final difference Fourier map was essentially featureless.

Final values of R and R_w (or wR_2) are included in Table 1.

2.3. Other measurements

IR spectra were recorded on KBr pellets using a Nicolet Nexus 670 spectrophotometer. Magnetic susceptibility data were collected in the 2.00–300 K range on powdered, microcrystalline samples on a Quantum Design MPMS-XL SQUID magnetometer equipped with a 7 T (70 kG) magnet. Diamagnetic corrections were applied to the observed paramagnetic susceptibilities using Pascal's constants.

3. Results and discussion

3.1. Synthesis

The comproportionation reaction of $Mn(OAc)_2\cdot 4H_2O$ with $KMnO_4$ in 60% aqueous acetic acid is the standard procedure for the preparation of $[Mn_{12}O_{12}(OAc)_{16}(H_2O)_4]$. We wondered whether this reaction in 60% methanolic acetic acid might instead yield a high nuclearity Mn–OMe–OAc cluster, especially given the recent report of the beautiful Mn_{21} cluster, $[Mn_{21}O_{24}(OMe)_8(O_2CCH_2Bu^t)_{16}(H_2O)_{10}]$ [15]. In fact, although the red–brown crystalline product was a new species, it did not contain MeO^- groups but was instead identified as polymeric $\{[Mn(OH)(OAc)_2]\cdot AcOH\cdot H_2O\}_n$ (**1**), a Mn^{III} species, isolated in non-optimized yields of ~16%. A white crystalline by-product is also sometimes formed and contaminates the crystals of **1**, but it can be removed by washing the mixture with MeOH.

$[Mn_{12}O_{12}(O_2CR)_{16}(H_2O)_4]$ chemistry was also to lead to another polymeric product. These Mn_{12} complexes have long been known to exhibit reversible oxidation and reduction processes when studied by, for example, cyclic voltammetry. In previous work, we have generated, isolated and studied both the one- and two-electron reduced versions, $[Mn_{12}O_{12}(O_2CR)_{16}(H_2O)_4]^{1-,\ 2-}$. [17–19] Using the R = Ph derivative, the generation and isolation of the one-electron oxidized species was attempted. Controlled potential electrolysis at +1.07 V versus ferrocene in CH_2Cl_2 appeared to proceed satisfactorily, but layerings with hexane did not cause crystallization of the expected red–brown oxidized species within a short timeframe, and the red–brown solution instead slowly changed color. We believe the oxidized species is generated, but it is a very strong oxidizing agent and more rapid precipitation/crystallization procedures will need to be developed to isolate the product before it decays. In the meantime, the slow color change was monitored, and it slowly converted from brown to purple, and eventually to the pale yellow

color diagnostic of Mn^{II} species. In some crystallization tubes, a little purple solid was obtained, and, in one case, well-formed purple crystals were obtained that permitted crystallographic study. This identified the deep purple product as polymeric $\{(NBu^n_4)[Mn_2(O_2PF_2)_6]\cdot 2/3CH_2Cl_2\}_n$ (**2**), a mixed-valent Mn^{II}/Mn^{III} material. The difluorophosphate groups presumably arise from hydrolysis of the PF_6^- ions of the supporting electrolyte, likely catalyzed by strongly oxidizing species generated as a result of the electrolysis and subsequent decay of the putative $[Mn_{12}]^+$ product. The formation of $F_2PO_2^-$ from PF_6^- has precedent [20–22]. Note that PF_6^- is often used without problems as the counter anion of cationic Mn_x complexes at Mn^{III} or higher oxidation states [23,24].

With the identity of **2** established, a more rational synthesis was sought. Treatment of $[Mn_{12}O_{12}(O_2CPh)_{16}(H_2O)_4]$ in CH_2Cl_2 with F_2PO_2H generates a deep purple solution, but attempts to isolate a purple solid were unsuccessful; the solution too rapidly fades to pale yellow. The fading can be slightly slowed down at low temperatures (−30 °C) and by exclusion of air.

The isolation of a new form of polymeric $Mn(OAc)_2$ and the subsequent structural characterization of $[Mn_4(OAc)_8(MeOH)_2]_n$ came about from a chance observation during a reaction using a solution of $Mn(OAc)_2\cdot 4H_2O$ in EtOH. There was a delay in adding a second reagent to this solution and a white precipitate was noticed forming in the hitherto clear solution. This was identified as a nearly anhydrous form of $Mn(OAc)_2$; solid filtered under nitrogen and dried in vacuo analyzed for $Mn(OAc)_2\cdot xH_2O$ with $x \approx 0.375$ (**3a**). Dried solid is air-stable but slightly hygroscopic, and prolonged exposure to air leads to analytical figures consistent with $x = 0.5$. Similar results are obtained in MeOH solution, except that Et_2O needs to be added to precipitate the product. In addition, methanolic solutions of $Mn(OAc)_2\cdot 4H_2O$ appear slightly air-sensitive giving the brown color of Mn^{III}, so anaerobic conditions were employed. However, reactions performed in air still give white precipitates, the brown species remaining in the filtrate. Powder obtained by rapid precipitation but stored in air analyzed for $Mn(OAc)_2\cdot H_2O$. Material grown as large crystals by slow crystallization and structurally characterized without being separated from mother liquor had a formulation $[Mn_4(OAc)_8(MeOH)_2]_n$ (**3b**). The MeOH groups (and by implication the H_2O groups in the hydrated solids) are bound to the Mn^{2+} ions (vide infra) and it is thus perhaps not surprising that in no case did we obtain strictly unsolvated $Mn(OAc)_2$.

Strictly anhydrous $Mn(OAc)_2$ (α form) has been reported from the dehydration of the tetrahydrate in refluxing $AcOH–Ac_2O$ (3:2) solution, followed by washing with Na-dried Et_2O and drying in vacuo [25]. Its structure has not been determined. Anhydrous $Mn(OAc)_2$ can also be obtained in two forms by a solvothermal procedure in MeCN at timescales from several hours to weeks [26]. Shorter timescales favor the α form, and longer ones favor a β form, which has been structurally characterized (vide infra) [27]. Thus, it was of interest to structurally characterize one of our forms of **3**, and crystals of **3b** proved suitable for this.

3.2. Structure of $\{[Mn(OH)(OAc)_2]\cdot AcOH\cdot H_2O\}_n$ (*1*)

Selected interatomic distances and angles are listed in Table 2. The compound contains a linear chain of repeating [Mn(μ-OH)(μ-OAc)$_2$Mn] units (Fig. 1), with each octahedral Mn^{III} atom lying on an inversion center. There are also mirror planes perpendicular to the chain axis and containing the OH^- group and the AcO^- carbon atoms. The chain of Mn atoms is thus exactly linear, and the bridging OH^- groups are *trans*. The Mn···Mn separations are 3.384 Å. All the AcO^- groups are in their familiar *syn*, *syn*-bridging modes. The Mn^{III} atoms exhibit a Jahn–Teller (JT) distortion, as expected for a d^4 ion in near-octahedral geometry, and it takes the form of an axial elongation (as is almost always the case for Mn^{III}). The JT-elongated axis is O(2)–Mn–O(2). It is interesting that the [Mn(μ-OH)(μ-OAc)$_2$Mn] triply-bridged unit is not known at the $2Mn^{III}$ oxidation level in a discrete dinuclear complex; such dinuclear species instead contain the [Mn(μ-O)(μ-OAc)$_2$Mn] core with a bridging oxide rather than hydroxide. It is likely that the trans disposition of the bridging O atoms in **1** is the explanation; the mutual trans influence of the μ-O atoms will weaken the Mn–O bonds and increase the basicity of these bridging O atoms, favoring their protonation. The [Mn(μ-OH)(μ-OAc)$_2$Mn] unit is

Table 2
Selected interatomic distances (Å) and angles (°) for $\{[Mn(OH)(OAc)_2]\cdot AcOH\cdot H_2O\}_n$ (**1**)

Bond lengths	
Mn···Mn	3.384
Mn–O1	1.898(1)
Mn–O3	1.936(2)
Mn–O2	2.176(2)
Bond angles	
O1–Mn–O1	180.00(13)
O1–Mn–O3	91.79(8)
O1–Mn–O3′	88.21(8)
O3–Mn–O3	180.00(12)
O1–Mn–O2′	87.38(7)
O3–Mn–O2′	88.54(6)
O1–Mn–O2	92.62(7)
O3–Mn–O2	91.46(6)
O2–Mn–O2	180.00(11)
Mn–O1–Mn	126.07(12)

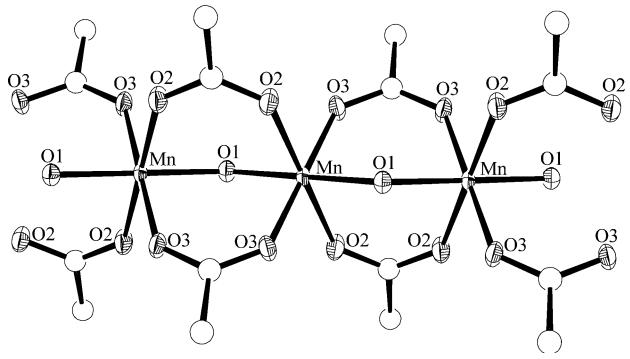

Fig. 1. An ORTEP plot at the 50% probability level of a small section of the polymeric chain of $\{[Mn(OH)(OAc)_2]\cdot AcOH\cdot H_2O\}_n$ (**1**).

known, however, in discrete form in $Mn^{II}Mn^{III}$ [28] and $Mn^{II}Mn^{II}$ [29] dinuclear species, consistent with the lower metal oxidation level.

The chains all run parallel in the crystal, and the presence of AcOH and H_2O solvent molecules of crystallization sets up a strong hydrogen-bonding network between chains. This is shown for a small section of two adjacent chains in Fig. 2. The inter-chain hydrogen-bonding comprises the μ-OH^- hydrogen-bonded to O5 of the AcOH molecule (O1···O5, 2.697(3) Å), whose OH group is hydrogen-bonded to the H_2O molecule (O4···O6, 2.548(4) Å). The latter hydrogen bonds to two O atoms from separate μ-OAc^- groups (O6···O2, 2.772(2) Å). The O···O distances and O–H···O angles (164(5)°–176(3)°) are indicative of strong hydrogen-bonds and help to favor **1** over molecular versions involving Mn_x ring structures or other topologies. A view down the chain axis is provided in Fig. 3, emphasizing the square channels occupied by solvent molecules.

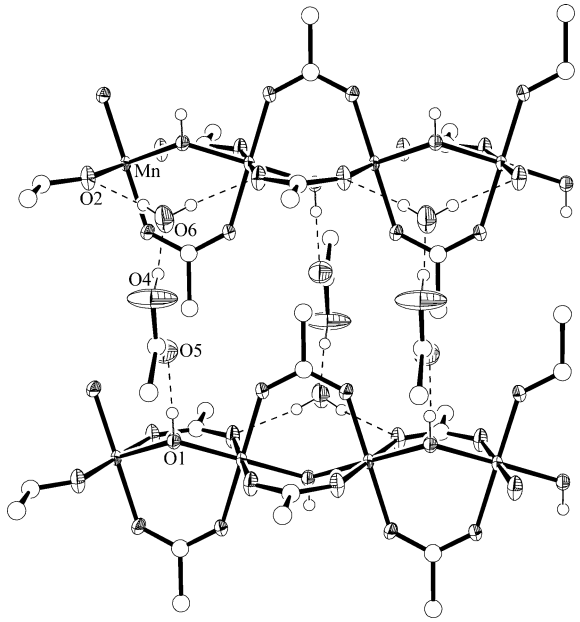

Fig. 2. A section of two adjacent chains of **1** illustrating the inter-chain hydrogen-bonding linkages through the AcOH and H_2O molecules.

3.3. Structure of $\{(NBu^n_4)[Mn_2(O_2PF_2)_6]\}_n$ (**2**)

Selected interatomic distances and angles are listed in Table 3. The compound is a chain polymer, with each pair of adjacent octahedral Mn atoms triply bridged by three $F_2PO_2^-$ groups (Fig. 4). Complex **2** is thus somewhat similar to **1** except that all bridging ligands are of the same type in the former. The asymmetric unit of **2** contains six inequivalent Mn atoms, a four-Mn segment of one chain and a two-Mn segment of an adjacent chain, and both are shown in Fig. 4.

Charge considerations clearly indicate that the compound is mixed-valence, and inspection of structural

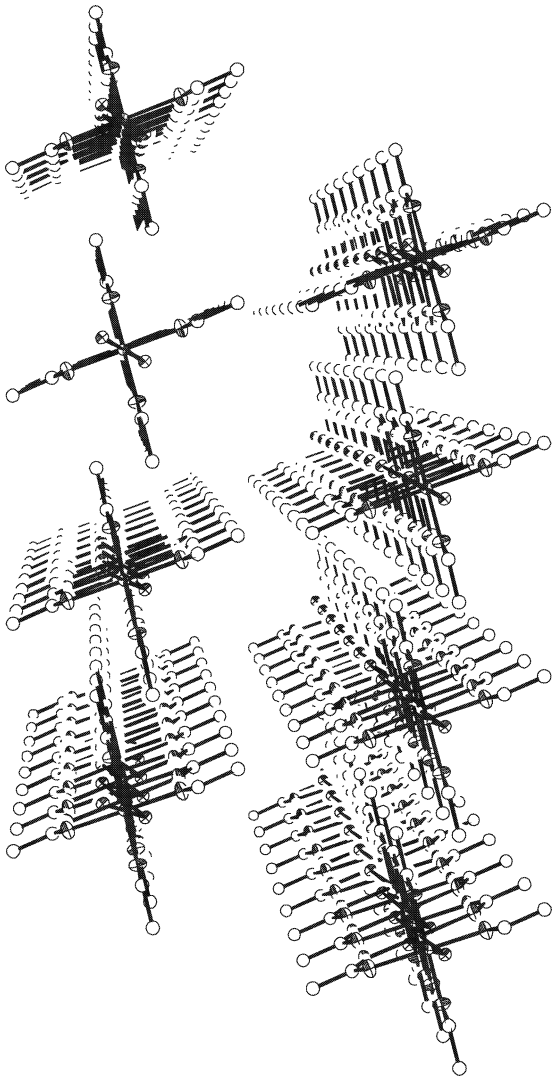

Fig. 3. A view along the chain axis of **1**.

Table 3
Selected interatomic distances (Å) and angles (°) for $\{(NBu^n_4)[Mn_2(O_2PF_2)_6]\cdot 2/3CH_2Cl_2\}_n$ (**2**)

Bond lengths			
Mn1···Mn2	4.759(2)	Mn3–O18	1.933(7)
Mn2···Mn3	4.813(2)	Mn3–O21	2.107(7)
Mn3···Mn4	4.757(2)	Mn3–O19	2.119(6)
Mn4···Mn1#1	4.805(2)	Mn4–O1#1	2.145(8)
Mn5···Mn6	4.764(2)	Mn4–O23	2.162(8)
Mn5···Mn6#1	4.737(2)	Mn4–O3#1	2.163(7)
Mn1–O7	1.916(7)	Mn4–O22	2.164(8)
Mn1–O9	1.919(6)	Mn4–O24	2.176(7)
Mn1–O8	1.962(7)	Mn4–O2#1	2.197(8)
Mn1–O6	1.965(6)	Mn5–O32	2.152(7)
Mn1–O5	2.062(6)	Mn5–O30	2.154(7)
Mn1–O4	2.114(6)	Mn5–O31	2.160(7)
Mn2–O14	2.127(8)	Mn5–O28	2.164(7)
Mn2–O15	2.159(7)	Mn5–O29	2.180(7)
Mn2–O10	2.165(7)	Mn5–O33	2.181(7)
Mn2–O12	2.178(8)	Mn6–O27#2	1.910(6)
Mn2–O11	2.184(7)	Mn6–O36	1.915(6)
Mn2–O13	2.196(8)	Mn6–O26#2	1.942(6)
Mn3–O16	1.901(7)	Mn6–O34	1.975(7)
Mn3–O20	1.914(7)	Mn6–O25#2	2.071(7)
Mn3–O17	1.926(7)	Mn6–O35	2.106(7)
Bond angles			
O7–Mn1–O9	179.1(3)	O1#1–Mn4–O23	89.9(3)
O7–Mn1–O8	91.5(3)	O1#1–Mn4–O3#1	90.4(3)
O9–Mn1–O8	87.9(3)	O23–Mn4–O3#1	96.1(3)
O7–Mn1–O6	90.4(3)	O1#1–Mn4–O22	90.6(3)
O9–Mn1–O6	90.2(3)	O23–Mn4–O22	88.3(3)
O8–Mn1–O6	177.7(3)	O3#1–Mn4–O22	175.5(3)
O7–Mn1–O5	85.8(3)	O1#1–Mn4–O24	178.6(3)
O9–Mn1–O5	93.5(3)	O23–Mn4–O24	88.7(3)
O8–Mn1–O5	91.3(3)	O3#1–Mn4–O24	89.8(3)
O6–Mn1–O5	90.2(3)	O22–Mn4–O24	89.3(3)
O7–Mn1–O4	89.5(3)	O1#1–Mn4–O2#1	91.5(3)
O9–Mn1–O4	91.2(3)	O23–Mn4–O2#1	176.6(3)
O8–Mn1–O4	89.6(3)	O3#1–Mn4–O2#1	87.0(3)
O6–Mn1–O4	89.1(3)	O22–Mn4–O2#1	88.6(3)
O5–Mn1–O4	175.3(3)	O24–Mn4–O2#1	90.0(3)
O14–Mn2–O15	92.5(3)	O32–Mn5–O30	173.3(3)
O14–Mn2–O10	91.2(3)	O32–Mn5–O31	92.2(3)
O15–Mn2–O10	88.8(3)	O30–Mn5–O31	94.5(3)
O14–Mn2–O12	177.8(3)	O32–Mn5–O28	91.8(3)
O15–Mn2–O12	89.3(3)	O30–Mn5–O28	89.1(3)
O10–Mn2–O12	87.6(3)	O31–Mn5–O28	89.3(3)
O14–Mn2–O11	91.5(3)	O32–Mn5–O29	87.7(3)
O15–Mn2–O11	88.6(3)	O30–Mn5–O29	91.6(2)
O10–Mn2–O11	176.4(3)	O31–Mn5–O29	89.6(3)
O12–Mn2–O11	89.8(3)	O28–Mn5–O29	178.7(2)
O14–Mn2–O13	86.2(3)	O32–Mn5–O33	86.1(3)
O15–Mn2–O13	178.7(3)	O30–Mn5–O33	87.2(3)
O10–Mn2–O13	90.8(3)	O31–Mn5–O33	177.5(3)
O12–Mn2–O13	92.0(3)	O28–Mn5–O33	88.8(3)
O11–Mn2–O13	91.8(3)	O29–Mn5–O33	92.2(3)
O16–Mn3–O20	92.3(3)	O27#2–Mn6–O36	175.6(3)
O16–Mn3–O17	178.6(3)	O27#2–Mn6–O26#2	91.1(3)
O20–Mn3–O17	87.6(3)	O36–Mn6–O26#2	89.1(3)
O16–Mn3–O18	90.2(3)	O27#2–Mn6–O34	90.0(3)
O20–Mn3–O18	177.5(3)	O36–Mn6–O34	89.9(3)
O17–Mn3–O18	89.9(3)	O26#2–Mn6–O34	178.1(3)
O16–Mn3–O21	88.6(3)	O27#2–Mn6–O25#2	91.7(3)
O20–Mn3–O21	90.8(3)	O36–Mn6–O25#2	92.6(3)
O17–Mn3–O21	92.8(3)	O26#2–Mn6–O25#2	92.8(3)
O18–Mn3–O21	89.5(3)	O34–Mn6–O25#2	85.7(3)
O16–Mn3–O19	90.1(3)	O27#2–Mn6–O35	86.1(2)
O20–Mn3–O19	91.2(3)	O36–Mn6–O35	89.6(3)
O17–Mn3–O19	88.6(3)	O26#2–Mn6–O35	92.1(3)
O18–Mn3–O19	88.6(3)	O34–Mn6–O35	89.5(3)
O21–Mn3–O19	177.7(3)	O25#2–Mn6–O35	174.7(3)

Symmetry transformations used to generate equivalent atoms: #1 $x, y, z-1$ #2 $-x+1, -y, z-1/2$ #3 $x, y, z+1$ #4 $-x+1, -y, z+1/2$.

parameters reveals a trapped-valence situation with Mn2, Mn4 and Mn5 being Mn^{II}, and Mn1, Mn3 and

Table 4
Selected interatomic distances and angles for $[Mn_4(OAc)_8(MeOH)_2]_n$ (**3b**)

Bond lengths			
Mn1–O5	2.167(12)	Mn3–O11	2.306(13)
Mn1–O9	2.139(13)	Mn3–O15	2.148(12)
Mn1–O13	2.144(15)	Mn3–O23	2.143(12)
Mn1–O17	2.157(14)	Mn3–O27	2.124(14)
Mn1–O21	2.229(12)	Mn3–O35	2.183(15)
Mn1–O25	2.222(12)	Mn4–O7	2.168(16)
Mn2–O11	2.188(12)	Mn4–O7	2.168(16)
Mn2–O19	2.128(13)	Mn4–O15	2.234(13)
Mn2–O21	2.256(12)	Mn4–O29	2.171(14)
Mn2–O25	2.221(12)	Mn4–O29	2.171(14)
Mn2–O31	2.138(13)	Mn4–O35	2.228(15)
Mn2–O33	2.160(14)	Mn4–O37	2.171(13)
Mn3–O9	2.320(13)	Mn4–O39	2.169(13)
Bond angles			
O5–Mn1–O9	93.2(5)	O9–Mn3–O27	82.2(5)
O5–Mn1–O13	92.0(5)	O9–Mn3–O35	166.5(5)
O5–Mn1–O17	83.6(5)	O11–Mn3–O15	166.4(5)
O5–Mn1–O21	172.4(5)	O11–Mn3–O23	86.3(5)
O5–Mn1–O25	96.9(4)	O11–Mn3–O27	84.6(5)
O9–Mn(1)–O13	90.5(5)	O11–Mn3–O35	116.3(5)
O9–Mn1–O17	90.1(5)	O15–Mn3–O23	90.4(5)
O9–Mn1–O21	91.5(5)	O15–Mn3–O27	96.8(5)
O9–Mn1–O25	169.8(5)	O15–Mn3–O35	77.3(5)
O13–Mn1–O17	175.5(6)	O23–Mn3–O27	168.4(5)
O13–Mn1–O21	93.9(5)	O23–Mn3–O35	104.9(5)
O13–Mn1–O25	87.3(5)	O27–Mn3–O35	85.6(5)
O17–Mn1–O21	90.5(5)	O7–Mn4–O5	100.3(5)
O17–Mn1–O25	92.9(5)	O7–Mn4–O29	92.9(5)
O21–Mn1–O25	78.6(4)	O7–Mn4–O35	166.5(5)
O11–Mn2–O19	91.1(5)	O7–Mn4–O37	85.9(5)
O11–Mn2–O21	169.6(5)	O7–Mn4–O39	92.6(5)
O11–Mn2–O25	93.0(4)	O15–Mn4–O29	164.3(5)
O11–Mn2–O31	96.3(5)	O15–Mn4–O35	74.7(4)
O11–Mn2–O33	84.7(5)	O15–Mn4–O37	97.0(5)
O19–Mn2–O21	94.3(5)	O15–Mn4–O39	84.8(5)
O19–Mn2–O25	89.7(5)	O29–Mn4–O35	94.2(5)
O19–Mn2–O31	83.3(5)	O29–Mn4–O37	92.4(5)
O19–Mn2–O33	173.6(5)	O29–Mn4–O39	86.1(5)
O21–Mn2–O25	78.1(4)	O35–Mn4–O37	82.4(5)
O21–Mn2–O31	93.3(5)	O35–Mn4–O39	99.3(5)
O21–Mn2–O33	90.7(5)	O37–Mn4–O39	177.8(6)
O25–Mn2–O31	168.5(5)	Mn1–O9–Mn3	08.2(6)
O25–Mn2–O33	95.3(5)	Mn2–O11–Mn3	105.0(5)
O31–Mn2–O33	92.4(5)	Mn3–O15–Mn4	104.5(5)
O9–Mn3–O11	56.8(4)	Mn1–O21–Mn2	95.2(5)
O9–Mn3–O15	109.9(5)	Mn1–O25–Mn2	96.3(5)
O9–Mn3–O23	86.7(5)	Mn3–O35–Mn4	103.5(5)

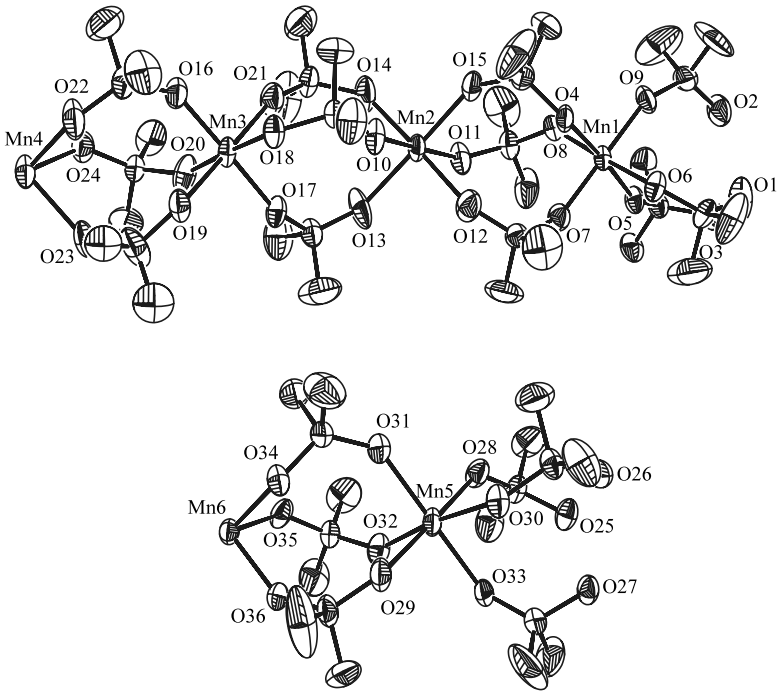

Fig. 4. An ORTEP plot at the 50% probability level of the crystallographically independent four-Mn and two-Mn sections of the polymeric chains of $\{(NBu^n_4)[Mn_2(O_2PF_2)_6]\}\cdot 2/3CH_2Cl_2\}_n$ (**2**).

Mn6 being Mn^{III}. Thus, the Mn^{II} and Mn^{III} ions alternate along the chain. As expected, the Mn^{II} ions have Mn–O bond lengths (2.127(8)–2.197(8) Å, av. 2.167 Å) that are significantly longer than the Mn^{III}–O ions (av. 1.987 Å). In fact, the latter also shows the expected JT axial elongation, as seen in **1**, with JT elongated bond lengths (2.062(6)–2.119(6) Å) noticeably longer than the rest (1.901(7)–1.975(7) Å). The JT axes in Fig. 4 are O4–Mn1–O5 and O19–Mn3–O21. The $Mn^{II}\cdots Mn^{III}$ separations are very long, in the range 4.757(5)–4.813(5) Å. As for **1**, the chains in **2** are all parallel, but there is no significant hydrogen-bonding either directly or with the CH_2Cl_2 molecules of crystallization. A view down the chain axis is shown in Fig. 5.

A number of complexes containing the $F_2PO_2^-$ group as a ligand are known; in almost all cases, it was obtained serendipitously by hydrolysis of PF_6^-, often in the presence of Ag^+, which is thought to catalyze the hydrolysis [22]. In Mn chemistry, the Mn^{II} complex $[Mn(O_2PF_2)_2]\cdot F_2PO_2H$ is known [30], as well as the Mn^{I} complexes $[Mn(CO)_5(O_2PF_2)]$ and $[Mn(CO)_3L_2(O_2PF_2)]$ ($L = PPh_3$, $P(OPh)_3$; $L_2 = bpy$) [31]. Complex **2** is thus the first structurally confirmed example of a Mn^{III}-containing species with this ligand.

3.4. Structure of $[Mn_4(OAc)_8(MeOH)_2]_n$ (**3b**)

Before consideration of the structure of $[Mn_4(OAc)_8(MeOH)_2]_n$, it is worthwhile to remember that common $Mn(OAc)_2\cdot 4H_2O$ also has a polymeric structure in the solid state [27]. This is depicted in Fig. 6. The structure contains linear trinuclear units that are linked by AcO^- bridges; the disposition of the latter is such as to give 2D polymeric sheets that are linked in the third dimension by a hydrogen-bonding network involving the bound and lattice H_2O groups. To emphasize the structure, $Mn(OAc)_2\cdot 4H_2O$ can be formulated as $\{[Mn_3(OAc)_4(OAc)_{4/2}(H_2O)_4]\cdot 8H_2O\}_n$. Selected interatomic distances and angles are listed in Table 4.

The structure of $[Mn_4(OAc)_8(MeOH)_2]_n$ (**3b**) consists of 1D chains of Mn_4 units that are linked by AcO^- bridges to yield a 3D polymer. The repeating unit of the chain can be formulated as $Mn_4(OAc)_5(OAc)_{6/2}$-$(MeOH)_2$. Its structure is shown in Fig. 7, where two units are shown to emphasize the inter-unit connections within a chain. The Mn_4 unit has a Y shape and is approximately planar (maximum deviation from the Mn_4 least-squares plane is 0.11 Å by Mn3). With the chains consisting of a line of Y-shaped Mn_4 units, they have an appearance not unlike a picket fence. The Mn atoms are linked by AcO^- groups in a variety of bridging modes (vide infra). Every Mn/Mn pair is bridged by three AcO^- groups except Mn3/Mn4, which is mono-atomically bridged by only two AcO^- groups. Inter-chain connections are by two AcO^- groups involving oxygen atoms O5/O7 and O29/O31. The two MeOH groups (O37 and O39) are terminally coordinated to Mn4. The relative alignment of the chains is shown in Fig. 8, a view along the chain; this view is perpendicular to that in Fig. 7. It can be seen that the chains are strongly connected by covalent linkages provided by the inter-chain bridging acetates. Thus, **3b**

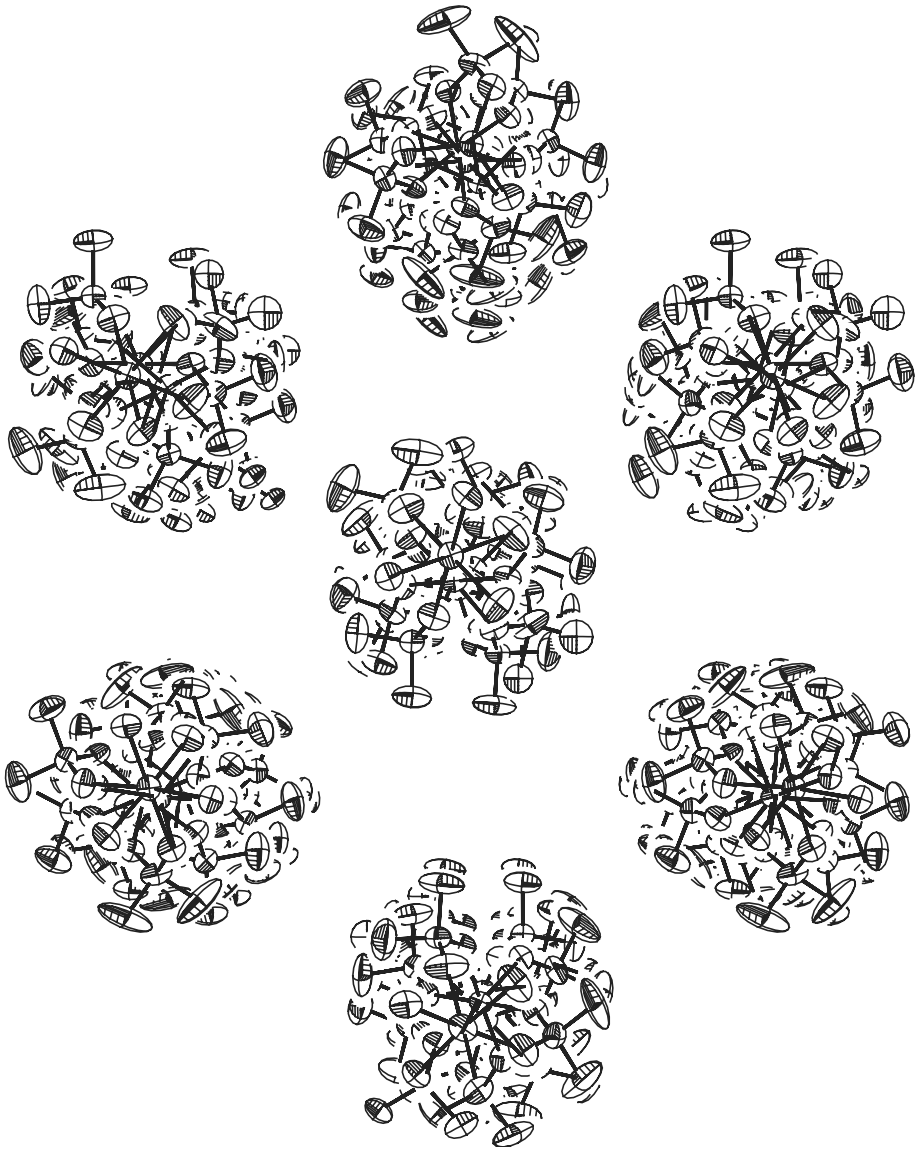

Fig. 5. A view along the chain axis of **2**.

truly is a 3D polymer. This is in contrast to $Mn(OAc)_2 \cdot 4H_2O$, where the linkages in one dimension are provided by hydrogen bonds to interstitial H_2O molecules, and the structure is best described as loosely-linked Mn acetate sheets.

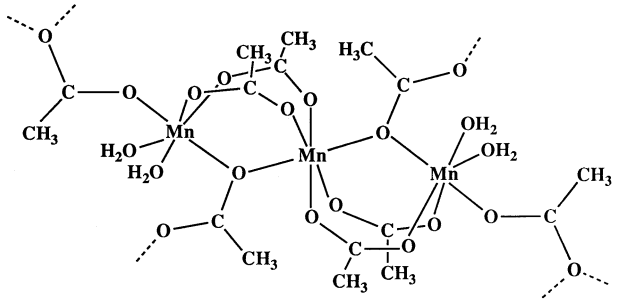

Fig. 6. The trinuclear unit within the polymeric structure of $Mn(OAc)_2 \cdot 4H_2O$.

It is interesting to consider the various types of acetate bridging mode found within **3b**; these are shown in Fig. 9. Type I is the common *syn*, *syn* μ-bridging mode, as also seen in **1**, and Type II is the somewhat rarer *syn*, *anti* mode. There are two μ_3-bridging modes: types III and IV are asymmetrically- and symmetrically-bridging modes, respectively.

3.5. Magnetochemistry of Compounds *1* and *3b*

Solid-state variable-temperature magnetic susceptibility (χ_M) studies were performed on a powdered sample of compound **1** in a 5 T (50 kG) field.

The data for **1** are plotted as $\chi_M T$ versus T in Fig. 10. The $\chi_M T$ value steadily decreases from 2.95 cm^3 K mol^{-1} at 300 K to 0.91 cm^3 K mol^{-1} at 15 K, and then

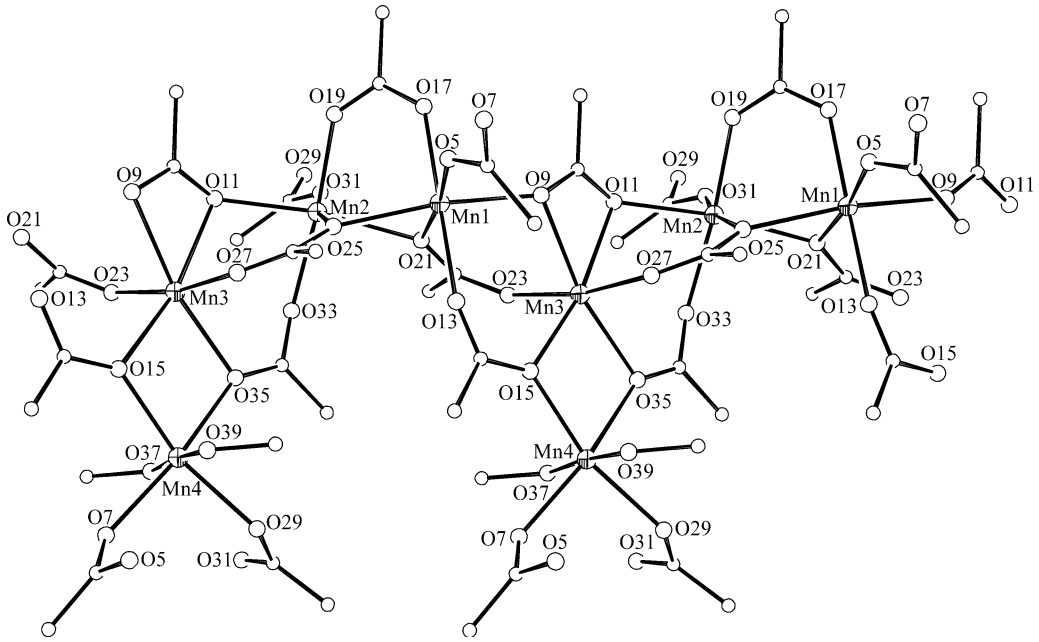

Fig. 7. A section of the polymeric chain of Y-shaped four-Mn units in $[Mn_4(OAc)_8(MeOH)_2]_n$ (**3b**).

steeply rises to 1.60 cm^3 K mol^{-1} at 6 K before decreasing sharply to 0.59 cm^3 K mol^{-1} at 2 K. The data indicate the Mn^{III} ions to be antiferromagnetically coupled within the chain. This is not surprising because triply-bridged Mn_2^{III} (and $Mn^{II}Mn^{III}$) dinuclear units are almost always antiferromagnetically-coupled, although a dinuclear complex with the $[Mn_2(\mu\text{-OH})(\mu\text{-OAc})_2]^{3+}$ core is not known for direct comparison. The low temperature behavior is suggestive of a weak ferromagnetic interaction between the chains, presumably mediated by the hydrogen-bonding network; the characterization of this low temperature behavior requires detailed study beyond the scope of the present paper.

Data were collected on both **3a** and **3b**, and those for the latter are plotted as $\chi_M T$ versus T in Fig. 11. Both complexes have very similar profiles, suggesting they possess the same structure. For **3b**, the $\chi_M T$ value

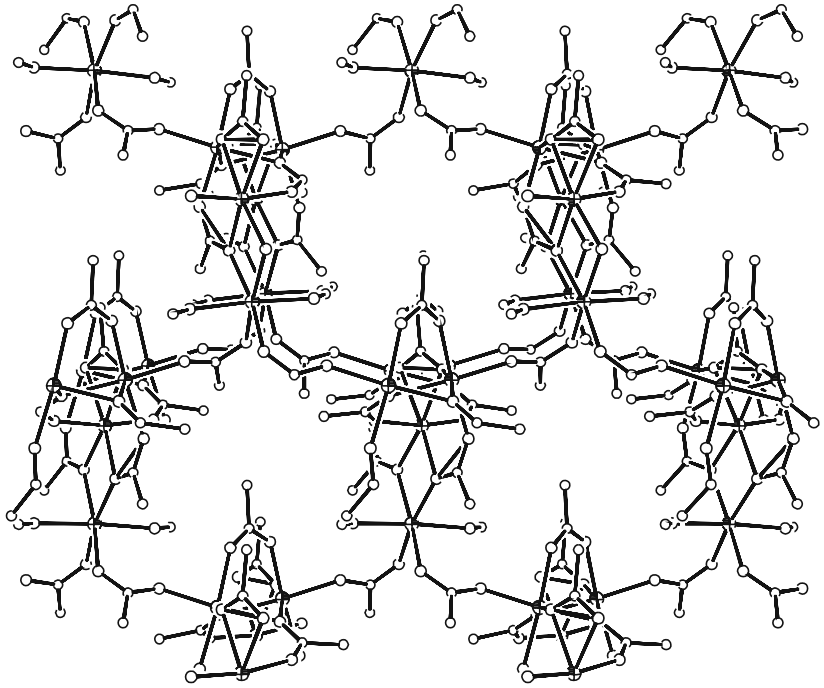

Fig. 8. A view along the chain axis of **3b** showing the inter-chain covalent linkages through the bridging AcO^- groups.

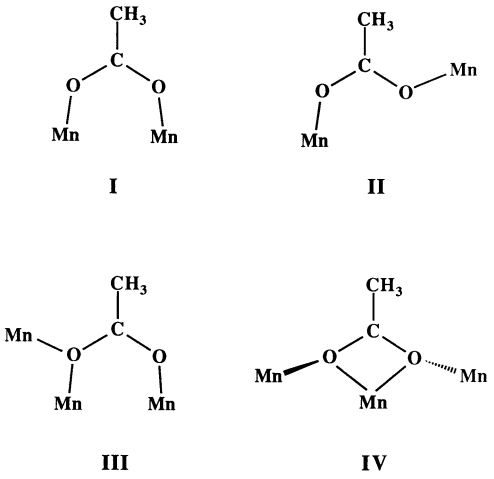

Fig. 9. The four types of AcO^- bridging mode in **3b**.

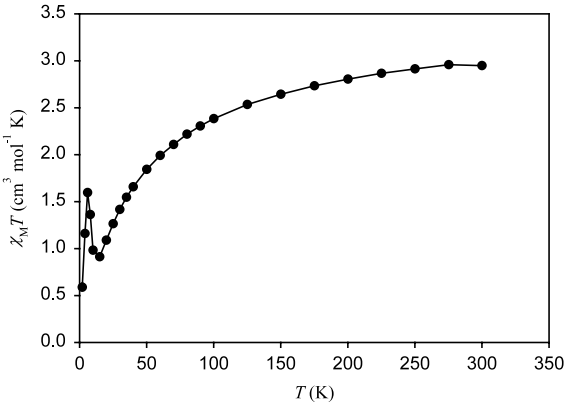

Fig. 10. A plot of $\chi_M T$ vs. T for $\{[Mn(OH)(OAc)_2]\cdot AcOH\cdot H_2O\}_n$ (**1**).

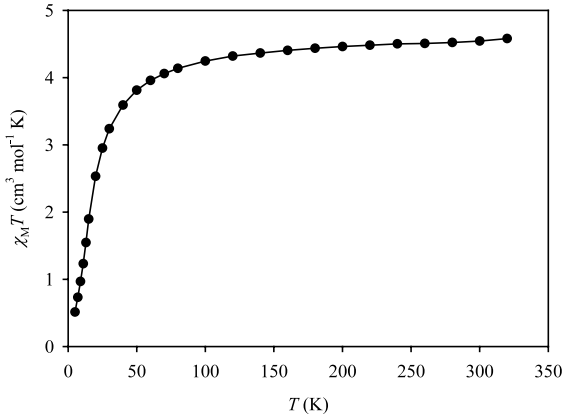

Fig. 11. A plot of $\chi_M T$ vs. T for $[Mn_4(OAc)_8(MeOH)_2]_n$ (**3b**).

steadily decreases from 4.58 cm^3 K mol^{-1} at 320 K to 0.51 cm^3 K mol^{-1} at 5.0 K. Again, the data indicate an overall antiferromagnetic coupling to give a diamagnetic ground state, as would be expected for a Mn^{II} system.

4. Conclusions

Three polymeric species have been obtained serendipitously. Two resulted from reactions related to or involving $[Mn_{12}O_{12}(O_2CR)_{16}(H_2O)_4]$ chemistry, and one resulted from a chance observation that an ethanolic solution of $Mn(OAc)_2\cdot 4H_2O$ slowly deposits a white microcrystalline powder. The three compounds are at different oxidation levels, Mn^{II}, mixed-valent Mn^{II}/Mn^{III}, and Mn^{III}, and thus provide a trio of species that permit interesting comparisons and contrasts.

The structures of the three polymers are similar to the extent that they all involve one-dimensional chains, but they differ in the degree of inter-chain linkages. The mixed-valent chains of $\{(NBu^n_4)[Mn_2(O_2PF_2)_6]\cdot 2/3CH_2Cl_2\}_n$ (**2**) are essentially non-interacting, being separated by CH_2Cl_2 molecules. In contrast, the chains of $\{[Mn(OH)(OAc)_2]\cdot AcOH\cdot H_2O\}_n$ (**1**) are linked by strong inter-chain hydrogen-bonds involving the AcOH and H_2O molecules. And finally, the chains in $[Mn_4(OAc)_8(MeOH)_2]_n$ (**3b**) are covalently bridged by AcO^- groups to give a true three-dimensional network.

Complex **2** is an unusual example of a mixed-valent Mn^{II}/Mn^{III} polymer, but its limited stability is unfortunate. The corresponding carboxylate analogue, $\{(NBu^n_4)[Mn_2(OAc)_6]\}_n$ is currently unknown but is being sought as a potentially more stable species that will allow detailed study of the properties (particularly magnetic) of such a mixed-valent chain.

The magnetic characterization of complexes **3a** and **3b** indicates the presence of antiferromagnetic interactions, giving a diamagnetic ground state. This is as expected for d^5 Mn^{II}. Intra-chain antiferromagnetic interactions also seem to be present in **1**, but the low-temperature $\chi_M T$ versus T data suggest that the inter-chain hydrogen bonding may mediate weak ferromagnetic interactions between the chains. More detailed studies of the low-temperature magnetic properties of **1** are required to assess this point further, and such studies are in progress.

5. Supplementary material

Crystallographic data in CIF format have been deposited at the Cambridge Crystallographic Data Center with CCDC numbers 189573 (**3b**), 189574 (**1**) and 189575 (**2**). Copies of this information may be obtained free of charge from The Director, CCDC, 12 Union Road, Cambridge, CB2 1EZ, UK (fax: +44-1223-336033; e-mail: deposit@ccdc.cam.ac.uk; or www: http://www.ccdc.cam.ac.uk).

Acknowledgements

This work was supported by the National Science Foundation.

References

[1] Photosynthetic water oxidation, J. Nugent (Ed.), Special Dedicated Issue Biochim. Biophys. Acta: Bioenerg. 1503 (2001) 1–259.
[2] V.K. Yachandra, K. Sauer, M.P. Klein, Chem. Rev. 96 (1996) 2927.
[3] J.B. Vincent, C. Christmas, H.-R. Chang, Q. Li, P.D.W. Boyd, J.C. Huffman, D.N. Hendrickson, G. Christou, J. Am. Chem. Soc. 111 (1989) 2086.
[4] G. Christou, Acc. Chem. Res. 22 (1989) 328.
[5] S. Wang, M.S. Wemple, J. Yoo, K. Folting, J.C. Huffman, K.S. Hagen, D.N. Hendrickson, G. Christou, Inorg. Chem. 39 (2000) 1501.
[6] S. Mukhopadhyay, R. Staples, W.H. Armstrong, Chem. Commun. (2002) 864.
[7] C. Philouze, G. Blondin, J.-J. Girerd, J. Guilhem, C. Pascard, D. Lexa, J. Am. Chem. Soc. 116 (1994) 8557.
[8] H.J. Eppley, S.M.J. Aubin, M.W. Wemple, D.M. Adams, H.-L. Tsai, V.A. Grillo, S. Castro, Z. Sun, K. Folting, J.C. Huffman, D.N. Hendrickson, G. Christou, Mol. Cryst. Liq. Cryst. 305 (1997) 167.
[9] G. Christou, D. Gatteschi, D.N. Hendrickson, R. Sessoli, MRS Bull. 25 (2000) 66.
[10] D.N. Hendrickson, G. Christou, H. Ishimoto, J. Yoo, E.K. Brechin, A. Yamaguchi, E.M. Rumberger, S.M.J. Aubin, Z. Sun, G. Aromi, Polyhedron 20 (2001) 1479.
[11] C. Boskovic, E. Brechin, W.E. Streib, K. Folting, J.C. Bollinger, D.N. Hendrickson, G. Christou, J. Am. Chem. Soc. 124 (2002) 3725.
[12] M. Soler, E. Rumberger, K. Folting, D.N. Hendrickson, G. Christou, Polyhedron 20 (2001) 1365.
[13] G. Aromi, S.M.J. Aubin, M.A. Bolcar, G. Christou, H.J. Eppley, K. Folting, D.N. Hendrickson, J.C. Huffman, R.C. Squire, H.-L. Tsai, S. Wang, M.W. Wemple, Polyhedron 17 (1998) 3005.
[14] W. Wernsdorfer, N. Aliaga-Alcalde, D.N. Hendrickson, G. Christou, Nature 416 (2002) 406.
[15] J.T. Brockman, J.C. Huffman, G. Christou, Angew. Chem., Int. Ed. Engl. 41 (2002) 2506.
[16] R. Sessoli, H.-L. Tsai, A.R. Schake, S. Wang, J.B. Vincent, K. Folting, D. Gatteschi, G. Christou, D.N. Hendrickson, J. Am. Chem. Soc. 115 (1993) 1804.
[17] H.J. Eppley, H.-L. Tsai, N. de Vries, K. Folting, G. Christou, D.N. Hendrickson, J. Am. Chem. Soc. 117 (1995) 301.
[18] M. Soler, S.K. Chandra, D. Ruiz, E.R. Davidson, D.N. Hendrickson, G. Christou, Chem. Commun. (2000) 2417.
[19] M. Soler, S.K. Chandra, D. Ruiz, J.C. Huffman, D.N. Hendrickson, G. Christou, Polyhedron 20 (2001) 1279.
[20] S. Mihan, K. Sünkel, W. Beck, Chem. Eur. J. 5 (1999) 745.
[21] G. Smith, D.J. Cole-Hamilton, A.C. Gregory, N.G. Gooden, Polyhedron 1 (1982) 97.
[22] R. Fernández-Galán, B.R. Manzano, A. Otero, J. Organomet. Chem. 577 (1999) 271.
[23] R. Hage, E.A. Gunnewegh, J. Niel, F.S.B. Tjan, T. Weyhermueller, K. Wieghardt, Inorg. Chim. Acta 268 (1998) 43.
[24] R.A. Reynolds, III, D. Coucouvanis, J. Am. Chem. Soc. 120 (1998) 209.
[25] D.A. Edwards, R.N. Hayward, Can. J. Chem. 46 (1968) 3443.
[26] J.D. Martin, R.F. Hess, Chem. Commun. (1996) 2419.
[27] E.F. Bertaut, T.Q. Duc, P. Burlet, M. Thomas, J.M. Moreau, Acta Crystallogr., Sect. B 30 (1974) 2234.
[28] A. Darovsky, V. Kezerashvili, P. Coppens, T. Weyhermuller, H. Hummel, K. Wieghardt, Inorg. Chem. 35 (1996) 6916.
[29] U. Bossek, K. Wieghardt, B. Nuber, J. Weiss, Inorg. Chim. Acta 165 (1989) 123.
[30] M.F.A. Dove, R.C. Hibbert, N. Logan, J. Chem. Soc., Dalton Trans. (1985) 707.
[31] F.L. Wimmer, M.R. Snow, Aust. J. Chem. 31 (1978) 267.